Kinetics of low pH–induced lamellar to bicontinuous cubic phase transition in dioleoylphosphatidylserine/monoolein

ARTICLE *in* THE JOURNAL OF CHEMICAL PHYSICS · APRIL 2011

Impact Factor: 2.95 · DOI: 10.1063/1.3575240 · Source: PubMed

4 AUTHORS, INCLUDING:

Toshihiko Oka
Shizuoka University
40 PUBLICATIONS **762** CITATIONS
SEE PROFILE

Noboru Ohta
SPring-8
10 PUBLICATIONS **117** CITATIONS
SEE PROFILE

Masahito Yamazaki
Shizuoka University
86 PUBLICATIONS **1,947** CITATIONS
SEE PROFILE

Kinetics of low *p*H-induced lamellar to bicontinuous cubic phase transition in dioleoylphosphatidylserine/monoolein

Mahay Md. Alam,[1,a)] Toshihiko Oka,[2,a)] Noboru Ohta,[3] and Masahito Yamazaki[1,2,b)]
[1]*Integrated Bioscience Section, Graduate School of Science and Technology, Shizuoka University, Shizuoka 422–8529, Japan*
[2]*Department of Physics, Faculty of Science, Shizuoka University, Shizuoka 422–8529, Japan*
[3]*Japan Synchrotron Radiation Research Institute/SPring-8, Hyogo 679–5198, Japan*

(Received 17 January 2011; accepted 16 March 2011; published online 12 April 2011)

Recently, it has been well recognized that the modulation of electrostatic interactions due to surface charges can induce transitions between lamellar liquid-crystalline (L_α) and inverse bicontinuous double-diamond cubic (Q_{II}^D) phases in biological lipids. To reveal their kinetic pathway and mechanism, we investigated the low *p*H-induced L_α to Q_{II}^D phase transitions in 20%-dioleoylphosphatidylserine (DOPS)/80%-monoolein (MO) using time-resolved small-angle x-ray scattering and a rapid mixing method. At a final *p*H of 2.6–2.9, the L_α phase was transformed completely into the hexagonal II (H_{II}) phase within 2–10 s after mixing a low *p*H buffer with a suspension of multilamellar vesicles of 20%-DOPS/80%-MO (the initial step). Subsequently, the H_{II} phase slowly converted into the Q_{II}^D phase and completely disappeared within 15–30 min (the second step). The rate constants of the second step were obtained using the singular value decomposition analysis. On the basis of these data, we discuss the underlying mechanism of the kinetic pathway of the low *p*H-induced L_α to Q_{II}^D phase transitions. © *2011 American Institute of Physics*. [doi:10.1063/1.3575240]

I. INTRODUCTION

Biomembranes and lipid membranes are usually in the lamellar liquid-crystalline (L_α) phase. However, under some conditions, lipids form nonlamellar phases such as the hexagonal II (H_{II}) and cubic (Q) phases. Recently, cubic phases of lipid membranes have attracted much attention in terms of both their biological and physicochemical characteristics.[1–3] The inverse bicontinuous cubic (Q_{II}) phase is an interesting family of cubic phases that includes the double-diamond Q_{II}^D (or Q^{224}), the Q_{II}^P (or Q^{229}), and the gyroid Q_{II}^G (or Q^{230}) phases. This family of phases has an infinite periodic minimal surface consisting of bicontinuous regions of water and hydrocarbon.[1] To date, the effects of temperature, water content, and pressure on the stability of the Q_{II} phases and the L_α/Q_{II} phase transitions have been investigated, but these severe physical conditions are generally lethal to cells. However, we identified a mild condition that induces these phase transitions via the electrostatic interactions due to the surface charges on lipid membranes. Specifically, as electrostatic interactions in the membrane interface increase in response to either an increase in the surface charge density of the membrane or a decrease in salt concentration, the most stable phase changes according to: $Q_{II}^D \Rightarrow Q_{II}^P \Rightarrow L_\alpha$.[4,5] Subsequently, other examples of the modulation of electrostatic interaction (EI)-induced L_α/Q_{II} phase transitions, and transitions between different Q_{II} phases in various lipids, were reported.[6–8] The addition of Ca^{2+}, Mn^{2+}, and positively charged peptides can induce the L_α to Q_{II} and the intercubic phase transitions in dioleoylphosphatidylglycerol (DOPG)/monoolein (MO) and other lipids, which can be explained by the decrease in the electrostatic interactions.[9–11] Recently, we found that low *p*H-induced transitions from the L_α to Q_{II}^D phase occur in dioleoylphosphatidylserine (DOPS)/monoolein within 1 h.[12] DOPS and MO are essential biological lipids, and *p*H is known to control the function and structure of membranes and proteins, thus playing an indispensable role in cells. These results demonstrate that the EI-induced L_α/Q_{II} phase transitions of biological lipids can be controlled by various mild factors, although their mechanisms of action are not well understood. However, it was recently recognized that cells can modulate the electrostatic interaction in membranes, and these modulations could play significant roles in controlling the structural changes occurring between cubic membranes and normal bilayers.[3]

To reveal the mechanism behind L_α/Q_{II} phase transitions, it is important to elucidate the kinetic pathway. Several researchers have investigated the kinetics of temperature (T) or pressure (P) jump-induced L_α to Q_{II} phase transition in various lipids using time-resolved small-angle x-ray scattering (TR-SAXS) and cryo-transmission electron microscopy (C-TEM).[13–18] For example, Seddon *et al*. investigated the T (or P) jump-induced L_α to Q_{II}^D phase transition in monoelaidin using TR-SAXS, and found that during the L_α to Q_{II}^D phase transition, a broad, featureless ring of scatter appeared. This then resolved itself into the intermediate Q_{II} phase with a larger lattice constant, and then gradually the lattice constant decreased with time.[15] Drummond *et al*. observed the regular arrangement of pores in membranes in T jump-induced L_α

a)These authors contributed equally.
b)Author to whom correspondence should be addressed. Electronic mail: spmyama@ipc.shizuoka.ac.jp. Tel./Fax: 81-54-238-4741.

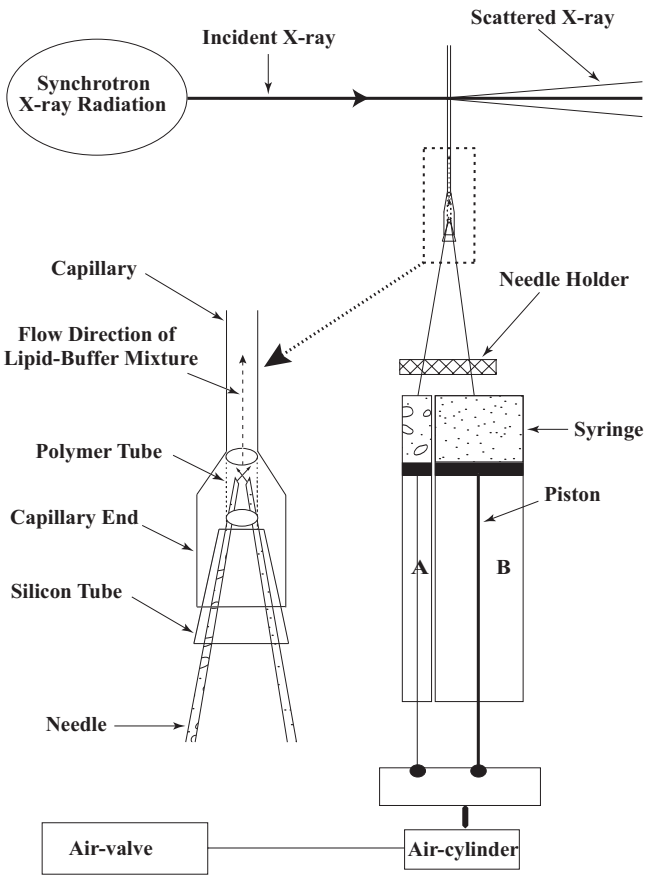

FIG. 1. The rapid mixing apparatus for SAXS measurements.

to Q_{II}^{D} phase transition in a synthetic lipid stabilized with a copolymer using C-TEM.[16] In protein science, TR-SAXS in combination with a rapid mixing system using the stopped-flow type have been used to follow rapid structural changes of proteins after a change of solution conditions.[19,20] Recently, Rappolt *et al*. applied this method to investigate the Ca^{2+}-induced L_α to H_{II} phase transition[21] and the Ca^{2+}-induced sponge (L3) to a mixture of Q_{II}^{D} and Q_{II}^{P} phase transition[22] in DOPG/MO using a combination of rapid mixing and TR-SAXS. They found that intermediate structures did not form during these phase transitions. These results indicate that TR-SAXS and C-TEM are useful for revealing the kinetic pathways of the phase transitions.

To reveal the mechanism behind the EI-induced L_α/Q_{II} phase transitions, it is important to elucidate their kinetics pathway. In this report, we investigated the kinetics of the low *p*H-induced L_α to Q_{II}^{D} phase transition in 20%-DOPS/80%-MO using TR-SAXS with synchrotron radiation and the home-made rapid mixing apparatus shown in Fig. 1. In this membrane system, large aggregates were formed following a decrease in *p*H. It was therefore not possible to use the standard stopped-flow apparatus previously described[19–22] because the aggregates blocked the narrow tubes in the apparatus. Using the new system depicted in Fig. 1 allowed the kinetic pathway of the low *p*H-induced L_α to Q_{II}^{D} phase transition in 20%-DOPS/80%-MO to be revealed.

II. MATERIALS AND METHODS

A. Materials

MO was purchased from Sigma Chemical Co. (St. Louis, MO, USA). DOPS was purchased from Avanti Polar Lipids (Alabaster, AL, USA). Poly (ethylene glycol) (PEG) with an average molecular weight of 7500 (PEG-6K) was purchased from Wako Pure Chemical Industry Ltd. (Osaka, Japan).

B. Preparation of membranes

To prepare dry lipid films, the appropriate amounts of MO in chloroform and DOPS in chloroform were mixed, then were dried first with N_2 gas and then under vacuum produced using a rotary pump (GCD-051X, ULVAC KIKO Inc., Miyazaki, Japan) for more than 12 h to remove the chloroform completely. For most experiments, the buffers contained 100 mM NaCl and 5% (w/v) PEG-6K. To prepare multilamellar vesicles (MLVs) of DOPS/MO membrane, 100 μl of 10 mM ammonium acetate buffer (*p*H 6.7) containing 100 mM NaCl and 5% PEG-6K (buffer A) was added to the dry MO/DOPS lipid film (10 μmol), and the suspension was mixed several times using a vortex mixer for about 30 s at room temperature (~25 °C). The DOPS/MO-MLVs in buffer A were used within 3 h of preparation.

All experiments were conducted in the presence of 5% (w/v) PEG-6K. As discussed previously,[12] the use of PEG-6K allows determination of the critical DOPS concentration and critical *p*H for inducing the L_α/Q_{II} phase transitions. Whereas DOPS/MO membranes in the absence of PEG-6K typically result in a mixture of Q_{II}^{D} and Q_{II}^{P} because the free energy of these phases is similar, the presence of a low concentration of PEG-6K stabilizes the Q_{II}^{D} phase preferentially over the Q_{II}^{P} phase.[11] This allows only the Q_{II}^{D} phase to be observed under conditions at which the Q_{II} phase appears, which makes the analysis of the SAXS patterns and the kinetics of the phase transitions much easier. It is well recognized that PEG-6K cannot interact with lipid membranes directly, and the decrease in the chemical potential of water due to the presence of PEG-6K plays important roles in the changes of physical properties of lipid membranes.[23,24] Large PEG-6K molecules are preferentially excluded from the inside of the lipid membrane–water system such as the Q phase-membrane mainly due to the steric hindrance, and thereby, at equilibrium the water content inside of the lipid membrane-water system is reduced to decrease the chemical potential of water inside the system, which should be equal to the chemical potential of water outside the system in the presence of PEG-6K. The decrease in the water content of the inside of the Q-phase membrane induces a decrease in its lattice constant, resulting in the change of the curvature elastic energy of the Q phase. Several theoretical studies have shown that, with decreasing water content, the most stable phase changes in the sequence that $Q_{II}^{P} \rightarrow Q_{II}^{D} \rightarrow Q_{II}^{G}$.[25] Moreover, in the presence of PEG-6K, the MLVs aggregate, which greatly increases the intensity of the SAXS peaks and thus the S/N of the SAXS peaks due to the lower content of water in the region where

the incident x-ray enters. This allows SAXS patterns with a high S/N to be obtained using a 2-s exposure time, without the need to accumulate additional data. Moreover, inside cells there are high concentrations of proteins, which decrease the chemical potential of water inside the cells and are preferentially excluded from the inside of the lipid membrane-water system. Thereby proteins in cells can play the same roles as PEG-6K as described above.[26] Therefore, the physical properties and phase behaviur of lipid membranes in the presence of PEG-6K may be more similar to those in the cells than those in the absence of PEG-6K.

C. SAXS measurements

The time-resolved SAXS data were measured at the BL40B2 beamline at SPring-8 (Sayo, Japan).[27] The x-ray wavelength used was 0.1000 nm and the camera length was 1116 mm. Data were collected using a CCD camera (C4742–98-24A, Hamamatsu Photonics, Hamamatsu, Japan) coupled with a 6-in. x-ray image intensifier (V5445P, Hamamatsu Photonics, Hamamatsu, Japan). A mixing system was used to mix rapidly a MLV suspension (in syringe A in Fig. 1) with a buffer (in syringe B in Fig. 1). This mixing system was controlled from outside the BL40B2 experimental hutch. An air-valve (062E1, Koganei Corporation, Koganei, Japan) regulated 0.2 MPa N_2 gas pressure to an air-cylinder (BDA10×30, Koganei Corporation, Koganei, Japan). The N_2 gas pushed both the piston of syringe A (25 μL, model 1702RN, Hamilton Company, Reno, NV, USA) and that of syringe B (250 μL, model 1725RN, Hamilton Company) simultaneously, which ejected the solution in syringe A and that in syringe B at the same speed instantaneously. The tips of the needles were placed in a short silicon tube that was connected to a quartz capillary. To inject the solutions smoothly into the capillary without formation of air bubbles, both ends of the capillary were open. A new capillary was used for each measurement to eliminate adherence of the lipid membranes to the capillary wall.

The suspension of DOPS/MO-MLVs (4 μl, 100 mM lipid concentration) in syringe A was rapidly mixed with 36 μl of 20 mM citrate buffer at various *p*H values containing 100 mM NaCl and 5% PEG-6K (buffer C) in syringe B, providing a final lipid concentration of 10 mM using the mixing system described above. The mixture was transferred directly into a 1.0-mm diameter quartz capillary (Mark tube, TOHO, Tokyo, Japan) (Fig. 1). The incident x-ray beam was adjusted onto the center of the white aggregates using the camera system. TR-SAXS measurements were made using 2-s exposures for the first 2 min and then 10-s exposures at various intervals or 10-s exposures at various intervals from the beginning at 25 °C ± 1 °C.

To measure the final *p*H of the DOPS/MO-MLV suspension mixed with the various citrate buffers (final lipid concentration 10 mM), a large volume (1–2 ml) of each mixture at a given ratio of MLV suspension to citrate buffer was prepared, the suspensions were centrifuged at 13 000 × *g* for 20 min at 25 °C using a MR-150 centrifuge (Tomy, Tokyo, Japan), then the *p*H of the supernatant was measured.[12]

D. Data analysis

A series of sequential two-dimensional ring diffraction patterns were averaged circularly to reduce them into a set of sequential one-dimensional patterns. These patterns were corrected by subtracting the background scattering caused by the capillary and buffer. Diffraction patterns for the singular value decomposition (SVD) analysis were normalized by the total intensity of each pattern to correct for intensity fluctuations caused by shifts in the sample in the x-ray beam. The sequential one-dimensional diffraction patterns are equivalent to a matrix $A(S, t)$, the matrix element A_{ij} of which corresponds to the intensity at the ith scattering vector S_i and jth delay-time t_j. Such an $m \times n$ matrix was decomposed with the SVD analysis[28–31] as

$$A(S,t) = U(S)S_{\mathrm{V}}V(t)^T,$$

where $U(S)$, S_{V}, and V are an $m \times n$ matrix, an $n \times n$ diagonal matrix, and an $n \times n$ matrix, respectively. The elements of matrix $U(S)$ describe the orthonormal basis spectra of $A(S, t)$. The values of the diagonal component in matrix S_{V}, called singular values, indicate the contribution of the basis spectra to $A(S, t)$. The components of $V(t)$ describe the time-dependent variation of the basis spectra. S_{V} are used as criteria to distinguish significant signals from noise.[28,29] The components of $V(t)$ with larger singular values determine the change of the SAXS pattern with time, and thereby we can neglect higher components of $V(t)$ with lower singular values. In our case, two significant components were extracted from the SVD analysis (see the details in Sec. III). The two extracted components of V, V_1, and V_2 were fitted with single exponential functions as: $V_i = \mathrm{c}_{i1} + \mathrm{c}_{i2} \exp[-kt]$, where $i = 1$ or 2. The rate constant k was set as a common parameter for V_1 and V_2. Using the values of the parameters obtained, the diffraction profiles of the decomposed components, B_1 and B_2, were reconstituted as $B_i = U_1 S_{\mathrm{V}1} \mathrm{c}_{1i} + U_2 S_{\mathrm{V}2} \mathrm{c}_{2i}$, where $i = 1$ or 2.

III. RESULTS

First, the kinetics of low *p*H-induced L_α to Q_{II}^D phase transition in 20%-DOPS/80%-MO (molar ratio) at a final *p*H of 2.6 was investigated. The SAXS pattern of 10 mM MLVs of this membrane in buffer A (*p*H 6.7) indicated that they were in the L_α phase with a spacing of 8.7 nm (Fig. 2). Immediately after the MLV suspension in buffer A was rapidly mixed with buffer C (*p*H 2.4), the MLVs in the resultant suspension (10 mM lipid, final *p*H of 2.6) associated with each other to produce white aggregates in the capillary. Figures 3(a) and 3(b) show the time course of the SAXS patterns of this sample. At 2 s after mixing, weak peaks with spacing in the ratio $1{:}\sqrt{3}{:}2$ appeared, corresponding to the H_{II} phase [Fig. 3(a)]. The intensities of these peaks increased with time up to 42 s. At 86 s, a weak, broad peak around $S = 0.125\ \mathrm{nm}^{-1}$ appeared with large peaks due to the H_{II} phase. The peaks with spacing in the ratio $\sqrt{2}{:}\sqrt{3}{:}\sqrt{4}{:}\sqrt{6}{:}\sqrt{8}{:}\sqrt{9}$, due to the Q_{II}^D phase [Fig. 4(a)], significantly increased with time, but the peaks due to the H_{II} phase decreased markedly and disappeared at 30 min [Fig. 3(b)]. Figure 4(b) shows the time course of the structural parameter of each phase. The

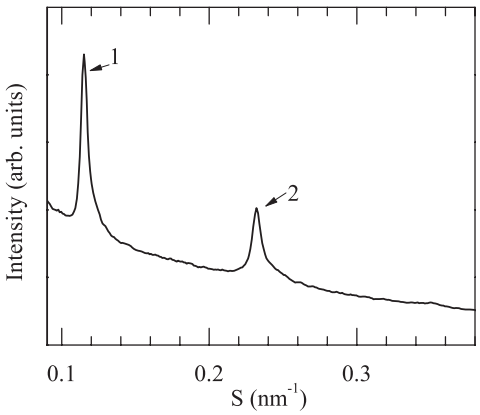

FIG. 2. A SAXS pattern of a 10 mM 20%-DOPS/80%-MO-MLV suspension in buffer A (*p*H 6.7); 10-s exposure time.

lattice constant of the Q_{II}^{D} phase gradually decreased with time. The kinetics of low *p*H-induced L_α to Q_{II}^{D} phase transition in the same lipid mixture at a final *p*H of 2.7 was very similar to that at *p*H 2.6, but the H_{II} phase disappeared at 20 min.

Second, the kinetics of low *p*H-induced phase transitions in the same lipid mixture at a final *p*H of 2.9 was investigated (Fig. 5). At 10 s after mixing, large peaks due to the H_{II} phase and small peaks due to the L_α phase appeared. The spacing of the L_α phase was the same as that of the original MLVs before mixing with the low *p*H buffer (Fig. 2), suggesting that some MLVs with larger diameter did not change structure or phase, perhaps because these MLVs are composed of many layered membranes (i.e., an onion structure) and thus H^+s could not penetrate the interior of these MLVs in a short time. At 22 s, only peaks due to the H_{II} phase were evident, and their intensities increased with time until 34 s. At 34 s, a weak, broad peak at $S = 0.125$ nm^{-1} appeared. Thereafter, the peaks with spacing in the ratio $\sqrt{2}:\sqrt{3}:\sqrt{4}:\sqrt{6}:\sqrt{8}:\sqrt{9}$ due to the Q_{II}^{D} phase (Fig. 5), and a peak around $S = 0.125$ nm^{-1}, significantly increased with time, but the peaks due to the H_{II} phase noticeably decreased and disappeared by 15 min. The peak at $S = 0.125$ nm^{-1} was ascribed to the L_α phase because at and above *p*H 3.2, the L_α phase appeared,[12] and the spacing of the MLVs in excess water decreased with a decrease in *p*H, presumably due to the decrease in electrostatic repulsion between neighboring membranes inside the MLVs. The *p*H value of 2.9 is critical, as it is the *p*H at which the L_α to Q_{II}^{D} phase transition occurred,[12] allowing both phases to coexist. The lattice constant of the Q_{II}^{D} phase gradually decreased with time.

Table I shows the lattice constants of the Q_{II}^{D} phase (the final equilibrium state) and the basis vector length (i.e., the distance between the centers of neighboring cylinders) a, of the H_{II} phases (the initial state) of 20%-DOPS/80%-MO at various low *p*H values. The lattice constants of the Q_{II}^{D} phase were very similar to those reported earlier,[12] indicating that the rapid mixing used in our experiments was successful. The value of a decreased with a decrease in *p*H. Generally, a is expressed as a sum of the distance between the center of the cylinder and the neutral surface (or pivotal surface), R_{pp}, and the distance between the bilayer midsurface and the neutral surface of the monolayer, ξ, i.e., $a = 2\ (R_{pp} + \xi)$. To allow the lipid monolayer in the H_{II} phase in excess water to adopt spontaneous curvature, H_0, the addition of alkanes such as tetradecane to the membranes is required, as these compounds can fill the interstitial region of the H_{II} phase and relax the hydrocarbon chain packing stress.[5,8] Under this condition, the curvature of the monolayer in the H_{II} phase is very close

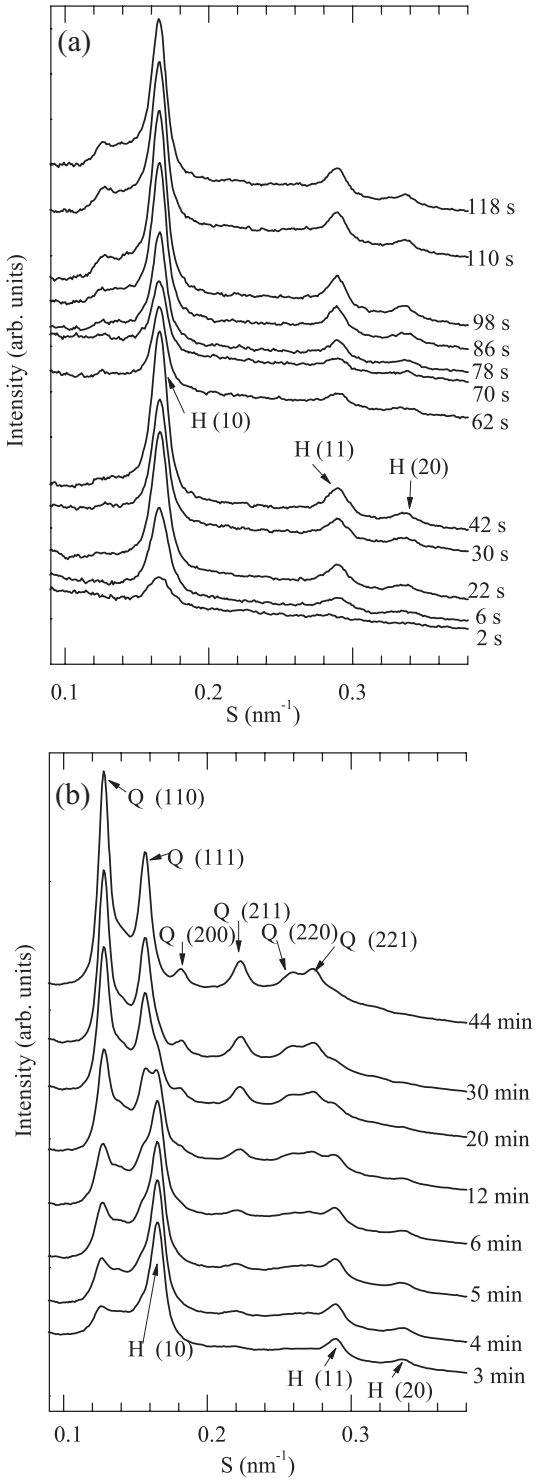

FIG. 3. Time course of the SAXS pattern of 20%-DOPS/80%-MO membranes after the *p*H of the suspension was adjusted to a final *p*H of 2.6. (a) From 2 to 118 s after the *p*H change; 2-s exposure time. (b) From 3 to 44 min after the *p*H change; 10-s exposure time.

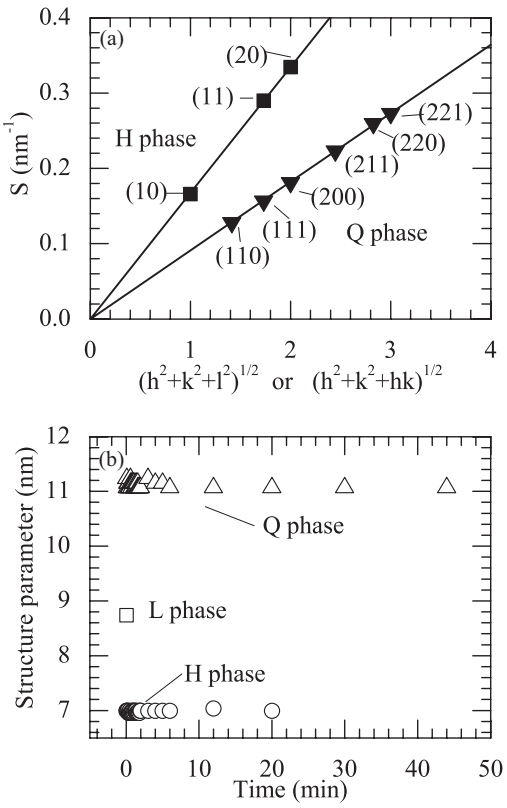

FIG. 4. (a) Indexing of the SAXS data of Fig. 3 at 44 min for the Q_{II}^{D} phase and 42 s for the H_{II} phase. The reciprocal spacing S (nm^{-1}) vs. $(h^2 + k^2 + l^2)^{1/2}$ (for the Q_{II}^{D} phase) or $(h^2 + k^2 + hk)^{1/2}$ (for the H_{II} phase) where h, k, and l are the Miller indices. (b) Time course of the structural parameter of the Q_{II}^{D}, the L_α, and the H_{II} phases of the SAXS data of Fig. 3.

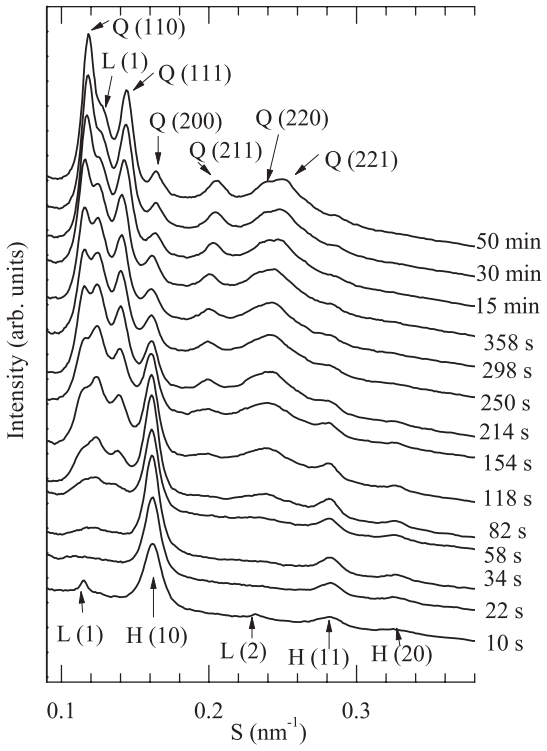

FIG. 5. Time course of the SAXS pattern of the 20%-DOPS/80%-MO after the *p*H of the suspension was adjusted to a final *p*H of 2.9; 10-s exposure time.

TABLE I. *p*H dependence of the structure parameter of 20%-DOPS/80%-MO membranes at (A) the equilibrium state and at (B) the initial state.

Final *p*H	(A) At equilibrium state lattice parameters for Q_{II}^{D} and L_α phases (nm)	(B) At initial state lattice parameter for H_{II} phase, a (nm)
2.9	12.0 (Q_{II}^{D}), 8.0 (L_α)	7.10
2.8	11.7 (Q_{II}^{D}), 7.7 (L_α)	7.05
2.7	11.4 (Q_{II}^{D})	6.99
2.6	11.0 (Q_{II}^{D})	6.92

to the spontaneous curvature, allowing the absolute value of the spontaneous curvature of a monolayer to be expressed as $|H_0| \approx 1/R_{pp}$. In this report we did not add alkanes to the DOPS/MO membranes, so the monolayer in the H_{II} phase could not adopt spontaneous curvature completely. However, the results shown in Table I indicate a decrease in R_{pp} with decreasing *p*H, suggesting that $|H_0|$ of this monolayer increases as the *p*H decreases. Moreover, the values of a in Table I are very similar to that of 20%-DOPS/80%-MO membrane containing 16 wt. % tetradecane in the same buffer at *p*H 2.8 (a = 7.0 nm), supporting that the phase in the initial state is the H_{II} phase.

To obtain quantitative information regarding this phase transition, the SAXS data were analyzed using the SVD analysis, which allows efficient extraction of information contained in a data set.[28] If diffraction patterns of different phases are overlapped, the patterns can be separated and their time course analyzed further with SVD. This feature is a powerful approach for analyzing diffraction patterns of transient mixed phases. Figures 6 and 7 show the results of SVD analysis for the SAXS pattern of the 20%-DOPS/80%-MO membrane after the *p*H of the suspension was adjusted to *p*H 2.6. The first

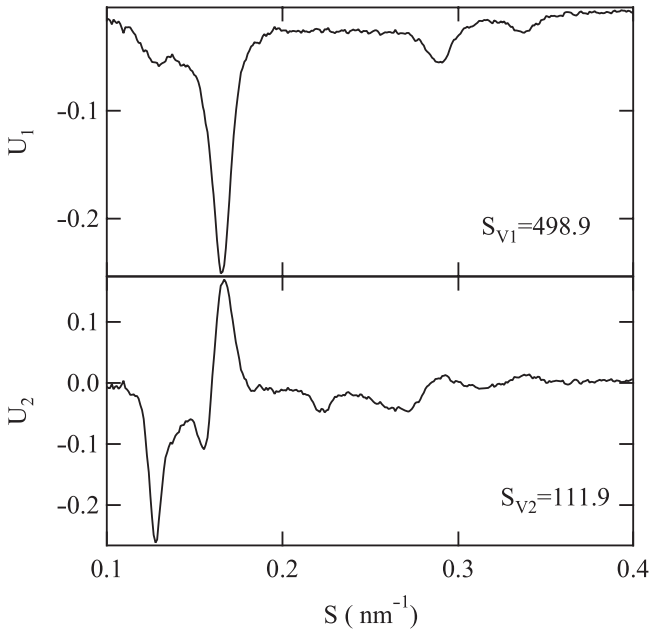

FIG. 6. *U* spectra of SVD analysis for the SAXS pattern of 20%-DOPS/80%-MO after the *p*H of the suspension was adjusted to a final pH of 2.6. The data show two major components with their singular values. Singular values of the third to seventh components are 19.7, 11.8, 9.5, 6.8, and 6.5.

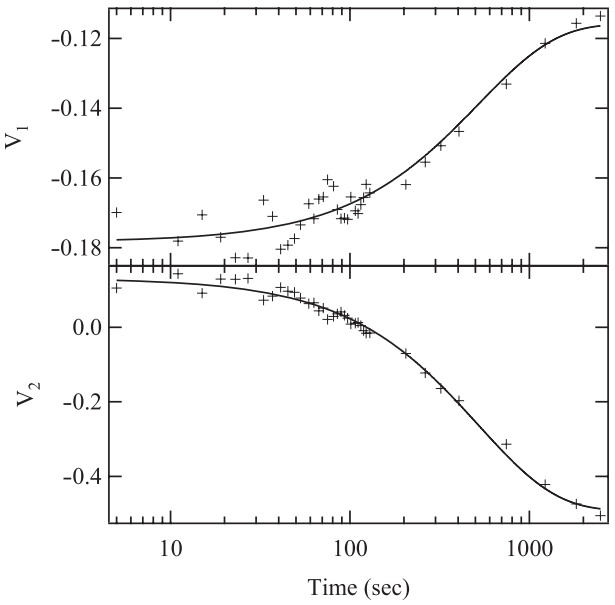

FIG. 7. *V* spectra of SVD analysis for the SAXS pattern of 20%-DOPS/80%-MO after the *p*H of the suspension was adjusted to a final *p*H of 2.6. These spectra indicate the time course of the corresponding *U* spectra in Fig. 6. Solid lines are the result of single exponential fitting.

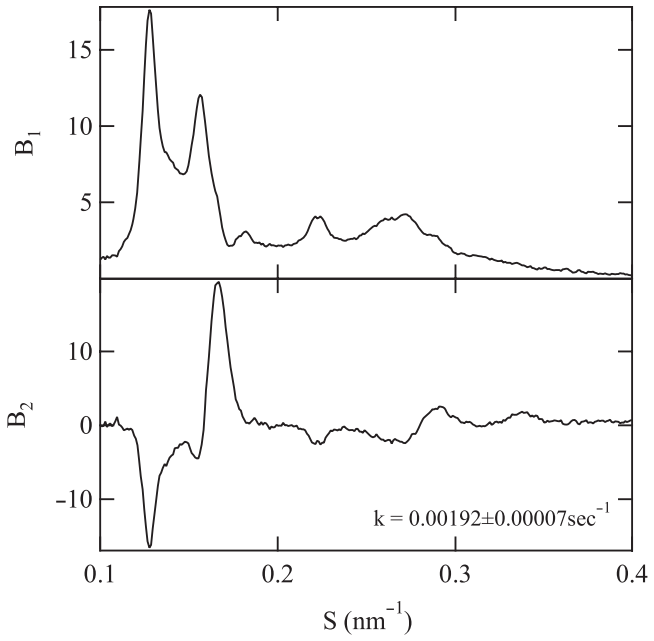

FIG. 8. Reconstituted *B* spectra from the SAXS pattern of 20%-DOPS/80%-MO after the *p*H of the suspension was adjusted to a final *p*H of 2.6. B_1 corresponds to the SAXS pattern of the final state. B_2 is a decay component with a rate constant, *k*.

two components are significant based on their singular values ($S_{V1} = 499$ and $S_{V2} = 112$, where S_{Vi} is the singular value of the *i*th component) and distinct *U* and *V*. Higher components, however, have lower singular values (e.g., $S_{V3} = 20$ and $S_{V4} = 12$, and other S_{Vi} values in Fig. 6 legend), which indicate less significance of the components. Thus, the higher components were omitted from further analysis. The existence of two significant components (first and second) indicates that two major states are involved in the kinetics of this low *p*H-induced phase transition. To analyze the time dependent change of the first and second components, we fitted V_1 and V_2 with single exponential functions, and the rate constant *k* was determined as $(1.9 \pm 0.1) \times 10^{-3}$ s^{-1} (Fig. 7). Both *V* spectra fit well to the functions. *B* spectra (Fig. 8) were reconstituted with *U* spectra and singular values and coefficients of the fit: B_1 corresponds to the SAXS pattern of the final state, and B_2 is a decay component with a rate constant, *k*. B_1 clearly corresponds to the pattern of the Q_{II}^D phase. B_2 is the difference SAXS pattern between the early component, the H_{II} phase, and the final component, B_1. Thus, the rate constant *k* corresponds to that of the phase transition from the H_{II} phase to the Q_{II}^D phase. Using the same method, we analyzed the kinetics data of the phase transition at a final *p*H of 2.7 and obtained very similar results, although B_1 corresponds to the Q_{II}^D phase and a small amount of the L_α phase. The rate constant of the phase transition at *p*H 2.7 was $(2.3 \pm 0.1) \times 10^{-3}$ s^{-1}, which is larger than that at *p*H 2.6. This is consistent with the result that the H_{II} phase disappeared sooner at *p*H 2.7 (i.e., 20 min) than at *p*H 2.6 (i.e., 30 min). At *p*H 2.8 and *p*H 2.9, which are the critical *p*H values of the phase transition between L_α and Q_{II}^D phases, both the phases appeared at the final stage (Table I). We therefore did not analyze the kinetics data at *p*H 2.8 and 2.9 using the SVD analysis since the interpretation of the analytical results would be difficult.

We can obtain the rate constant of the H_{II} to the Q_{II}^D phase transition *k* using the analysis of the time courses of the peak intensities under some assumptions. Using this analysis we obtained almost the same value of the rate constant as that obtained using the SVD analysis (see the details in the Appendix). We discuss the advantages and disadvantages of the peak intensity analysis and the SVD analysis in the Appendix.

IV. DISCUSSION

The above results clearly show the kinetic pathway of the low *p*H-induced L_α to Q_{II}^D phase transition: first, the L_α phase converts into the H_{II} phase in immediate response to the *p*H change, then the H_{II} phase gradually converts into the Q_{II}^D phase. The initial step is rapid and is complete in less than 2–10 s, in contrast the second step, which is slow and takes 15–30 min. We analyzed the kinetics of the second step quantitatively using the SVD analysis, and obtained the rate constant *k* of the H_{II} to Q_{II}^D phase transition. However, the kinetics of the first step could not be analyzed quantitatively due to the low time resolution of the apparatus used.

The mechanism of the low *p*H-induced L_α to Q_{II} phase transition can be analyzed from an equilibrium point of view. As discussed previously,[5,8] the electrostatic interaction-induced L_α to Q_{II} phase transition is controlled mainly by the curvature elastic energy of the monolayer f_{curv} due to the change in the spontaneous curvature of monolayer H_0. Generally, f_{curv} can be expressed as[32]

$$f_{curv} = \int \{2\kappa_m(H^\xi - H_0)^2 + \overline{\kappa}_m K^\xi\} dA^\xi, \quad (1)$$

where κ_m is the elastic bending modulus of the monolayer, H^ξ is the mean curvature at the neutral surface of the monolayer, K^ξ is the Gaussian curvature at the neutral surface, and $\bar{\kappa}_m$is the Gaussian curvature modulus of the monolayer; the integration extends over the monolayer's neutral surface, which is at a distance ξ from the midsurface of the bilayer (i.e., the parallel surface). Using the geometric characteristics of the L_α and the cubic phases, the difference between the free energy of cubic phase F_Q and that of the L_α phase $F_{L\alpha}$, $\Delta F_{Q\text{-}L}$, can be obtained from [8,32,33]

$$\Delta F_{Q-L} = F_Q - F_{L\alpha} = \bar{\kappa}_{bil}\langle K\rangle A, \tag{2}$$

where $\langle K\rangle$ is the average value of the Gaussian curvature of the membrane over its total neutral surface area A, and $\bar{\kappa}_{bil}$ is the Gaussian curvature modulus of the bilayer

$$\bar{\kappa}_{bil} = 2(\bar{\kappa}_m - 4\kappa_m H_0 \xi). \tag{3}$$

Equation (2) shows that $\Delta F_{Q\text{-}L}$ is determined by the value of $\bar{\kappa}_{bil}$, since $\langle K\rangle < 0$; if $\bar{\kappa}_{bil} > 0$ the Q_{II} phase is more stable, and the L_α/Q_{II} phase transition occurs at $\bar{\kappa}_{bil} = 0$.[8,32,33] Equation (3) shows that $\bar{\kappa}_{bil}$ greatly depends on the value of H_0 of the monolayer; when H_o has a large negative value (i.e.,$|H_0|$ is large), $\bar{\kappa}_{bil} > 0$ since $\bar{\kappa}_m < 0$,[32] indicating that the Q_{II} phase is more stable. Moreover, we found experimentally that an increase in electrostatic interactions due to the surface charges of membranes significantly reduces $|H_0|$ of the monolayer.[5,8,9] If we assume that the electrostatic interactions do not change $\bar{\kappa}_m$ and κ_m greatly, we can consider the following scenario.[5,8] As the electrostatic interactions due to surface charges of a membrane decrease, $|H_0|$ of the monolayer increases, inducing an increase in $\bar{\kappa}_{bil}$. At the critical value of the electrostatic interactions, $\bar{\kappa}_{bil} = 0$, and the L_α to Q_{II} phase transition occurs. Below the critical value of the electrostatic interactions, $\bar{\kappa}_{bil} > 0$ and the Q_{II} phase is more stable. In the above mechanism, we neglect the electrostatic interaction energy between neighboring membranes,[8] the lamellar phase unbinding energy,[34] and the fourth-order curvature energy,[35] all of which may play a role in the L_α/Q_{II} phase transition. As discussed previously,[12] in the low *p*H-induced L_α to Q_{II} phase transition, a decrease in the *p*H of the membrane suspension decreases the surface charge density of the DOPS/MO membrane due to protonation of the carboxylic acid of DOPS, which in turn induces an increase in $|H_0|$ of the monolayer. This mechanism is supported by the results of the *p*H dependence of the basis vector length of the H_{II} phase (Table I). Thus, as the *p*H decreases $\bar{\kappa}_{bil}$ increases, and at the critical *p*H ($= pH_Q$) $\bar{\kappa}_{bil} = 0$, and thereby the L_α to Q_{II} phase transition occurs. The pH_Q values for the low *p*H-induced L_α to $Q_{II}{}^D$ phase transition in 20%-DOPS/80%-MO and 25%-DOPS/75%-MO are *p*H 2.9 and *p*H 2.7, respectively.[12] The pK_a^{app} of the DOPS carboxylic acid was also obtained experimentally by assuming that the L_α/Q_{II} phase transition is controlled only by the surface charge density of the membrane. This pK_a^{app} value agreed with the theoretical value of its pK_a^{app} obtained analyzing the effects of the electrostatic interactions and dielectric constant of the membrane interface.[12] The above results substantiate our conclusion that the low *p*H-induced L_α to Q_{II} phase transition is controlled mainly by electrostatic interactions associated with the surface charge density of the membrane.

On the other hand, the difference between the free energy of the H_{II} phase F_H and that of the L_α phase $F_{L\alpha}$, $\Delta F_{H\text{-}L}$ can be described by[36]

$$\Delta F_{H-L} = F_H - F_{L\alpha} = \left(\mu_{ch} - 4\kappa_m H_0^2\right) A, \tag{4}$$

where μ_{ch} is the packing energy of hydrocarbon chains per unit area of the neutral surface in the interstitial region of the H_{II} phase, which is always positive (i.e., $\mu_{ch} > 0$). Equation (4) shows that $\Delta F_{H\text{-}L}$ is determined by the value of H_0: if $|H_0| > \sqrt{\mu_{ch}/4\kappa_m}$ the H_{II} phase is more stable, and the L_α/H_{II} phase transition occurs at $|H_0| = \sqrt{\mu_{ch}/4\kappa_m}$. As described above, in the low *p*H-induced L_α to H_{II} phase transition, as the *p*H decreases $|H_0|$ increases and at the critical *p*H ($= pH_H$), $|H_0| = \sqrt{\mu_{ch}/4\kappa_m}$, where the L_α to H_{II} phase transition occurs. The value of pH_H for the low *p*H-induced L_α to H_{II} phase transition in 25%-DOPS/75%-MO is *p*H 2.4, which is lower than its pH_Q value.[12] The value of pH_H for the phase transition in 20%-DOPS/80%-MO could not be determined because we could not decrease the *p*H of the membrane suspension below *p*H 2.4 due to the characteristics of the citrate buffer.

As described above, from an equilibrium point of view, the most stable phase of the DOPS/MO membrane changes with a decrease in *p*H according to $L_\alpha \rightarrow Q_{II}{}^D \rightarrow H_{II}$. Therefore, the difference between the free energy of the $Q_{II}{}^D$ phase and the H_{II} phase is not large. This is similar to the temperature dependence of the most stable phase of various lipid membranes: with an increase in temperature, $L_\alpha \rightarrow Q_{II}{}^D \rightarrow H_{II}$. We next considered the kinetics of the low *p*H-induced L_α to Q_{II} phase transition. At the *p*H region where the free energy of the Q_{II} phase is minimum among the three phases (i.e., L_α, H_{II}, and $Q_{II}{}^D$) (Fig. 9), the $Q_{II}{}^D$ phase is formed at equilibrium. However, the kinetics pathway of phase transitions is governed by the rate constant, which is determined by the activation energy (or the energy barrier) of the transitions of the structural changes. There may be several elementary steps between the two phases. In this case the slowest elementary step among all the elementary steps, i.e., the rate-determining step, governs the total rate of the phase transition. Thereby if we compare the rate constants of the rate-determining steps of different kinetic pathways, the most probable pathway can be identified. As shown in Fig. 9, if the activation energy of the rate-determining step in one kinetic pathway (i.e., the L_α to $Q_{II}{}^D$ phase transition) is much larger than that in the other kinetic pathway (i.e., the L_α to H_{II} phase transition), the L_α phase first transforms into the H_{II} phase and then converts to the $Q_{II}{}^D$ phase. In contrast, if the activation energy of the rate-determining step in the L_α to H_{II} phase transition is much larger than that in the L_α to $Q_{II}{}^D$ phase transition, the L_α phase transforms directly into the $Q_{II}{}^D$ phase. It is note that the rate constant also depends on the attempt frequency (e.g., the pre-exponential factor in the Arrhenius equation of the rate constant), and thereby the difference in the attempt frequency of the rate-determining step of both the pathways may determine the kinetic pathway.

It is instructive to compare the kinetics of the low *p*H-induced L_α to Q_{II} phase transition with that of T

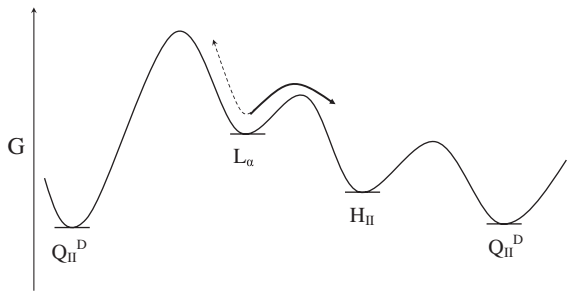

FIG. 9. The proposed kinetic pathway for the low *p*H-induced L_α to Q_{II}^D phase transition. There may be several elementary steps between the two phases, but the rate-determining step governs the total rate of the phase transition. This figure shows only the rate-determining steps in the L_α to Q_{II}^D phase transition and the L_α to H_{II} phase transition.

change-induced L_α to Q_{II} phase transition. To date, it has been believed that during the L_α to H_{II} phase transition, the Q_{II} phases appear as intermediate structures when temperature is increased.[37,38] However, several exceptions have been reported. Caffrey *et al.* found that in T-jump experiments conducted with *N*-monomethylated dioleoylphosphatidylethanolamine (DOPE-Me), a metastable H_{II} phase formed initially and disappeared very slowly while the Q_{II} phase developed; after 3 h incubation, both phases coexisted.[17] The kinetics pathway for this system may be similar to that of our DOPS/MO system, although the rate constant of the L_α to Q_{II}^D phase transition in our system is much larger than that of the T-jumped transition. Tenchov *et al*. observed the formation of the Q_{II} phase by temperature cycling across the transition temperature between the L_α and H_{II} phases.[39] These results indicate that there is high activation energy for the L_α/Q_{II} phase transitions. Siegel *et al*. pointed out that the T change-induced transition from L_α to nonlamellar phases such as Q_{II} and H_{II} phases is determined by kinetic factors.[40,41] In the DOPE-Me membrane, the rate of the L_α to Q_{II} and the L_α to H_{II} phase transitions are in kinetic competition.

The above results provide a basis for understanding the mechanism underlying the kinetic pathway of the low *p*H-induced L_α to Q_{II} phase transition. There are several theories regarding the stability of various Q_{II} and L_α phases or phase sequences in lipids,[25,42] but currently there is no quantitative theory of kinetics for the L_α/Q_{II} phase transition in lipids. A qualitative theory explaining the kinetics pathway of the T change-induced L_α to Q_{II} phase transition in various lipids has been proposed by Siegel *et al*.; their model is consistent with the stalk hypothesis and their observations using a C-TEM[33,40,41] (see Fig. 1 in Ref. 41). Thermal fluctuation of bilayers in the L_α phase induces contacts with neighboring bilayers, the apposed (*cis*) monolayers fuse to form stalk structures [Fig. 1(b)],[41] and the *trans*- monolayers contact (TMC) or hemifusion intermediate is produced [Fig. 1(c)].[41] There are two patterns of structural changes from the TMC. If the *trans* monolayers at the TMC rupture, an interlamellar attachment (ILA) or a fusion pore [Fig. 1(d)] [41] is formed (Type A). If ILAs accumulate in sufficient numbers, they form ILA lattices, which are intermediates in Q_{II} phase formation. If rupture does not occur and the TMC accumulation and aggregate, the H_{II} phase appears (Type B). The bilayer rupture tension τ^* may determine the relative rate of H_{II} phase formation.[41] Membranes with large values of τ^* favor H_{II} phase formation (i.e., the rate of H_{II} phase formation is larger than that of ILA production and hence Q_{II} phase formation). In other words, in membranes with large values of τ^*, the activation energy of the rate-determining step from the L_α to Q_{II}^D phase transition is much larger than that from the L_α to H_{II} phase transition (Fig. 9). If we assume that the 20%-DOPS/80%-MO membrane has a large value of τ^*, this hypothesis can explain the results of the kinetics pathway of the low *p*H-induced L_α to Q_{II}^D phase transition.

Finally, we consider the second step of the low *p*H-induced L_α to Q_{II}^D phase transition: the H_{II} to Q_{II}^D phase transition. The H_{II} phase gradually transforms into the Q_{II}^D phase because the free energy of the Q_{II}^D phase is smaller than that of the H_{II} phase, due to a positive Gaussian curvature elastic modulus of the bilayer. However, the kinetics pathway and mechanism are not known. In the SAXS patterns shown in Figs. 3(a) and 5(a), a weak, broad SAXS peak is present around $S = 0.125\ \mathrm{nm}^{-1}$, appearing at the beginning of the H_{II} to Q_{II}^D phase transition. This peak may be due to the Q_{II}^D phase or to an intermediate structure such as ILA arrays.

Further analysis will require quantitative theories and computer simulations for the low *p*H-induced lamellar to bicontinuous cubic phase transition in lipids.

V. CONCLUSION

This report investigated the kinetics of the low *p*H-induced L_α to Q_{II}^D phase transition in 20%-DOPS/80%-MO using TR-SAXS with synchrotron radiation and the rapid-mixing method. Decreasing the *p*H to 2.6–2.9 caused the L_α phase to completely transform into the H_{II} phase within 2–12 s, then the H_{II} phase slowly converted into the Q_{II}^D phase with time. Finally, the H_{II} phase completely converted into the Q_{II}^D phase (i.e., the transition was complete) in less than 15–30 min; the time required depended on the final *p*H. Moreover, we obtained the rate constant of the H_{II} to Q_{II}^D phase transition using the SVD analysis. Based on these experimental results, we demonstrated for the first time the presence of an intermediate in the electrostatic interaction-induced L_α to Q_{II} phase transition.

ACKNOWLEDGMENTS

This work was supported by a grant-in-aid for Scientific Research in Priority Areas (Soft Matter Physics) (Grant No. 21015009) from the Ministry of Education, Culture, Sports, Science and Technology (MEXT) of Japan and by a grant-in-aid for Scientific Research (B) (Grant No. 17310071) from the Japan Society for the Promotion of Science (JSPS) to M.Y. The synchrotron radiation experiments were performed at the BL40B2 in the SPring-8 with the approval of the Japan Synchrotron Radiation Research Institute (JASRI) (Proposal No. 2009B1222, 2010A1198). Preliminary results were obtained at BL-10C of the Photon Factory (Tsukuba, Japan), under the approval of the Photon Factory Advisory Committee (Proposal No. 2009G516). This work was partially carried out

using an instrument at the Center for Instrumental Analysis of Shizuoka University.

APPENDIX: COMPARISON BETWEEN THE PEAK INTENSITY ANALYSIS AND THE SVD ANALYSIS

To determine the rate constant k of the H_{II} to the Q_{II}^{D} phase transition in the second step of the low *p*H-induced the L_{α} to Q_{II}^{D} phase transition, here we used a different method from the SVD one. We analyzed the time course of the SAXS peak intensities of the 20%-DOPS/80%-MO membrane after the *p*H of the suspension was adjusted to *p*H 2.6 (Fig. 3). First, the peak intensities of H_{II} (10) and Q_{II}^{D} (110) at each time were obtained by integrating the area of the peak shown in Fig. 10(a). Then, we plotted the time courses of the peak intensities [Fig. 10(b)], which are almost the same as the V spectrum of the SVD analysis (Fig. 7). The time courses were well fitted with the same single exponential functions as those used in the analysis of the V spectrum, and the rate constant k, which was set as the common parameter for both time courses, was determined as $(1.7 \pm 0.1) \times 10^{-3}$ s^{-1}. The value of k is almost the same as that determined using the SVD analysis ($(1.9 \pm 0.1) \times 10^{-3}$ s^{-1}). We also analyzed time courses of 5 peak intensities of H_{II} (10), H_{II} (11), Q_{II}^{D} (110), Q_{II}^{D} (111), and Q_{II}^{D} (211), using the same method. The results show that all the curves were well fitted with the common rate constants k, whose value is the same as the above value of k. It strongly supports that this rate constant is for the H_{II} to the Q_{II}^{D} phase transition.

Both the analysis methods (the above peak intensity analysis and the SVD analysis) gave us the same value of the rate constant of the H_{II} to the Q_{II}^{D} phase transition. Here it is useful to compare both the methods. The peak intensity analysis seems to be an easier method than the SVD one, because it is more straightforward and intuitive without using the matrix algebra. However, it has several disadvantages as follows. To obtain peak intensity, we have to define the peak area at first. When a few peaks are overlapped (in our case, the H_{II} (10) peak was overlapped with the Q_{II}^{D}(111) peak, shown in Fig. 10(a), the peak intensity of one phase is affected by the overlapped peak of another phase, and thereby the accuracy of the peak intensity is low. If we assume that the change of the SAXS pattern occurs due to the two-state transition, this problem does not affect the result significantly. But this indicates that the peak intensity analysis needs such an assumption. In the analysis of three-state transitions with overlapped peaks and that of a transition with a lattice constant shift, this problem induces a substantial error in the determination of the rate constants. If we use a software to separate overlapping peaks into the sum of several Lorenzian peaks, it is possible to eliminate the effect of the overlapping.[14] However, it is a very time-consuming work to do this kind of peak fitting of many SAXS patterns obtained by TR-SAXS.

In contrast, the SVD analysis itself does not need any hypothesis such as the two-state transition for the analysis of the SAXS patterns, because it is a simple matrix calculation and does not need preprocesses which might affect data quality. Moreover, the result of the SVD analysis provides us another useful information.[28] Based on the values of S_V vector obtained by the SVD analysis, we can determine, without any assumptions, the number of the components in data, i.e., the number of the states in the phase transition in our case, which is one of the most important steps to analyze data with a proper transition model. For example, if there are two significant components, the two states are involved in the transition. If a transition model is built, we can fit the model to the V spectrum (Fig. 7), and reconstitute SAXS profiles of components in the model, such as B spectrum in Fig. 8. The reconstituted profiles help us to judge the model we built is correct or not. Therefore, the SVD analysis has several advantages that help us to build an appropriate model of a transition.

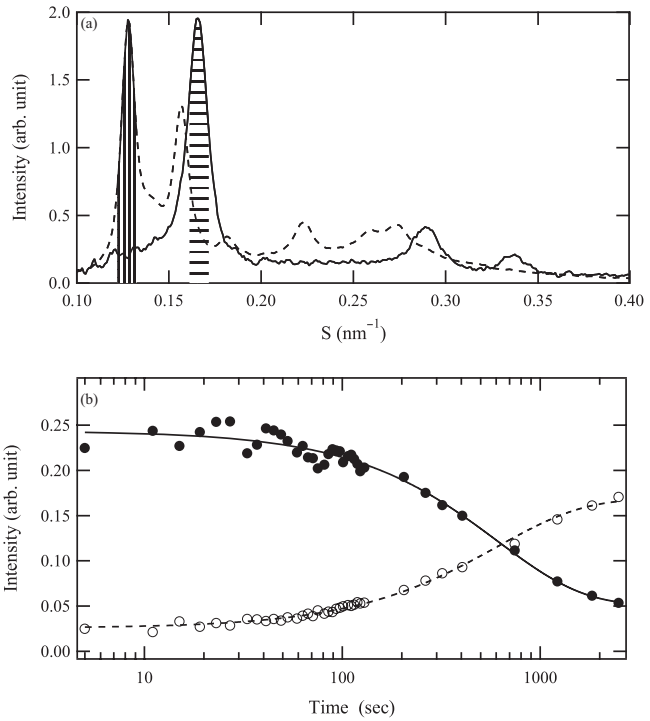

FIG. 10. (a) SAXS pattern of the 20%-DOPS/80%-MO membrane after the *p*H of the suspension was changed into the final *p*H 2.6 at 42 s (solid line) and 44 min (dashed line). To determine the SAXS peak intensities of H_{II} (10) and Q_{II}^{D} (110) at each time, a shaded area with horizontal lines in the H_{II} (10) peak and that with vertical lines in the Q_{II}^{D} (110) peak are integrated, respectively. (b) Time course of the peak intensity of H_{II} (10) (closed circle) and Q_{II}^{D} (110) (open circle). Solid and dashed lines are the best fitting curve with single exponential functions whose rate constant was set as a common parameter for both the data. The rate constant is $(1.7 \pm 0.1) \times 10^{-3}$ s^{-1}.

On the basis of the above comparison, we can select the method to analyze data of TR-SAXS. When the number of the states in a phase transition is well known and there is no overlapping of SAXS peaks of different states, we can use the peak intensity analysis. On the other hand, when the number of the states in the phase transition is unknown (case 1) or in the analysis of three-state transitions with overlapped peaks (case 2) and that of a transition with a lattice constant shift (case 3), we had better use the SVD analysis. Our case in this paper corresponds to the case 1, because we did not know the number of the states in the phase transition before the analysis.

[1]J. M. Seddon and R. H. Templer, in *Structure and Dynamics of Membranes*, edited by R. Lipowsky and E. Sackmann (Elsevier, Amsterdam. 1995), vol. 97.
[2]V. Luzzati, Curr. Opin. Struct. Biol. **7**, 661 (1997).
[3]Z. A. Almsherqi, S. D. Kohlwein, and Y. Deng, J. Cell Biol. **173**, 839 (2006).
[4]Y. Aota-Nakano, Y. Yamashita, S. J. Li, and M. Yamazaki, Biochim. Biophys. Acta **1461**, 96 (1999).
[5]S. J. Li, Y. Yamashita, and M. Yamazaki, Biophys. J. **81**, 983 (2001).
[6]V. Cherezov, J. Clogston, Y. Misquitta, W. Abdel-Gawad, and M. Caffrey, Biophys. J. **83**, 3393 (2002).
[7]V. Chupin, J. A. Killian, and B. de Kruijff, Biophys. J. **84**, 2373 (2003).
[8]M. Yamazaki, Adv. Planar Lipid Bilayers Liposomes **9**, 163 (2009).
[9]T. S. Awad, Y. Okamoto, S. M. Masum, and M. Yamazaki, Langmuir **21**, 11556 (2005).
[10]M. Pisani, V. Fine, P. Bruni, E. D. Cola, and O. Francescangeli, J. Phys. Chem. B **112**, 5276 (2008).
[11]S. M. Masum, S. J. Li, T. S. Awad, and M. Yamazaki, Langmuir **21**, 5290 (2005).
[12]Y. Okamoto, S. M. Masum, H. Miyazawa, and M. Yamazaki, Langmuir **24**, 3400 (2008).
[13]J. Kraineva, R. A. Narayanan, E. Kondrashkina, P. Thyagarajan, and R. Winter, Langmuir **21**, 3559 (2005).
[14]A. M. Squires, R. H. Templer, J. M. Seddon, J. Woenckhaus, R. Winter, S. Finet, and N. Theyenchei, Langmuir **18**, 7384 (2002).
[15]C. E. Conn, O. Ces, X. Mulet, S. Finet, R. Winter, J. M. Seddon, and R. H. Templer, Phys. Rev. Lett. **96**, 108102 (2006).
[16]X. Mulet, X. Gong, L. J. Waddington, and C. J. Drummond, ACS Nano **3**, 2789 (2009).
[17]V. Cherezov, D. P. Siegel, W. Shaw, S. W. Burgess, and M. Caffrey, J. Membr. Biol. **195**, 165 (2003).
[18]B. Angelov, A. Angelova, U. Vainio, V. M. Garamus, S. Lesieur, R. Willumeit, and P. Couvreu, Langmuir **25**, 3734 (2009).
[19]T. Ueki, Y. Hiragi, M. Kataoka, Y. Inoko, Y. Amemiya, Y. Izumi, H. Tagawa, and Y. Muroga, Biophys. Chem. **23**, 115 (1985).
[20]M. Arai, T. Ikura, G. V. Semisotnov, H. Kihara, Y. Amemiya, and K. Kuwajima, J. Mol. Biol. **275**, 149 (1998).
[21]A. Yaghmur, P. Logger, B. Sartori, and M. Rappolt, PLoS ONE **3**, e2072 (2008).
[22]A. Yaghmur, B. Sartori, and M. Rappolt, Phys. Chem. Chem. Phys. **13**, 3115 (2011).
[23]M. Yamazaki, S. Ohnishi, and T. Ito, Biochemistry **28**, 3710 (1989).
[24]M. Yamazaki, M. Ohshika, N. Kashiwagi, and T. Asano, Biophys. Chem. **43**, 29 (1992).
[25]U. S. Schwarz and G. Gompper, Phys. Rev. Lett. **85**, 1472 (2000).
[26]A. Suzuki, M. Yamazaki, and T. Ito, Biochemistry **28**, 6513 (1989).
[27]K. Inoue, T. Oka, K. Miura, and N. Yagi, AIP Conf. Proc. **705**, 336 (2004).
[28]E. R. Henry and J. Horfrichter, Methods Enzymol. **210**, 129 (1992).
[29]T. Oka, N. Yagi, T. Fujisawa, H. Kamikubo, F. Tokunaga, and M. Kataoka, Proc. Natl. Acad. Sci. U.S.A. **97**, 14278 (2000).
[30]T. Oka, K. Inoue, M. Kataoka, and N. Yagi, Biophys. J. **88**, 436 (2005).
[31]D. I. Svergun and M. H. J. Koch, Rep. Prog. Phys. **66**, 1735 (2003).
[32]U. S. Schwarz and G. Gompper, Langmuir **17**, 2084 (2001).
[33]D. P. Siegel and M. M. Kozlov, Biophys. J. **87**, 366 (2004).
[34]D. P. Siegel and G. Tenchov, Biophys. J. **94**, 3987 (2008).
[35]D. P. Siegel, Langmuir **26**, 8673 (2010).
[36]D. Marsh, Biophys. J. **70**, 2248 (1996).
[37]J. Briggs and M. Caffrey, Biophys. J. **66**, 573 (1994).
[38]R. N. A. H. Lewis, R. N. McElhaney, P. E. Harper, D. C. Turner, and S. M. Gruner, Biophys. J. **66**, 1088 (1994).
[39]B. Tenchov, R. Koynova, and G. Rapp, Biophys. J. **75**, 853 (1998).
[40]D. P. Siegel and R. M. Epand, Biophys. J. **73**, 3089 (1997).
[41]D. P. Siegel, Biophys. J. **76**, 291 (1999).
[42]W. B. Lee, R. Mezzenga, and G. H. Fredrickson, Phys. Rev. Lett. **99**, 187801 (2007).